Supporting Information

Neuman et al. 10.1073/pnas.0900574106

SI Text

Support for a Large Nearly Orthogonal Preferred Crossing Angle. In agreement with previous reports (1, 2), we show that yeast topoisomerase II (Topo II) preferentially relaxes DNA segments juxtaposed at 90° (Fig. 2). Given the high degree of structural and functional homology between yeast Topo II and *Escherichia coli* Topo IV (3), it seems unlikely that the two enzymes would adopt radically different DNA-binding geometries. Moreover, in vivo, both topoisomerases are thought to be responsible primarily for the decatenation of linked DNA, which is favored by a preferred crossing angle closer to 90°.

The value of $\alpha_0 \approx 85°$ we obtained is surprisingly close to the symmetric value of 90°, for which there would be no difference in relaxation rates. Indeed, Monte Carlo (MC) simulations (4, 5) suggest that for $\alpha_0 \approx 85°$, (+)sc DNA would be relaxed ≈2-fold faster than (−)sc DNA, significantly less than the previously measured ratio of at least 20 (4, 6, 7). Although our finding of a large nearly symmetric preferred crossing angle was surprising, it is consistent with the observation that Topo IV binds and unlinks plasmid dimers more efficiently than it relaxes (+)sc DNA (8). Simulations of positively catenated dimers (Fig. S1) indicate a broad distribution of crossing angles peaked slightly >90° (4). Simulations of (+)sc DNA, however, indicate a narrower distribution of crossing angles peaked near 60° (5). The fact that Topo IV binds and relaxes positively catenated DNA more efficiently than (+)sc DNA (8) suggests that the probability of obtaining the preferred crossing angle is higher for positively catenated than for (+)sc DNA, which is consistent with a preferred crossing angle close to 90°.

Comparison of Processivity Model with Previous Measurements of Relaxation Rate Asymmetry for Topo IV. As a consistency check of the processivity model (see main text and Fig. S4*A*), we compared the calculated and measured asymmetry parameters from the supercoil relaxation measurements. Relaxation asymmetry was measured for 8 supercoils ($n = 8$) with an average binding time (t_b) of ≈20 s and a cycle time (t_c) of 0.4 s (7). Under these conditions, the calculated value of $R = 21 \pm 3$ agrees with the measured value of 21 ± 3. As an additional check of the model, we computed the expected asymmetry parameter from previous single-molecule measurements, which were unable to measure the relaxation of both positive and negative supercoils at the same Topo IV concentration. Crisona et al. (6) measured the relaxation of 30 positive supercoils. Assuming an average waiting time $<t_b> \approx 50$ s, the computed asymmetry parameter $R = 74 \pm 8$ (Fig. S4*A*), corresponding to a time of approximately 1 h to relax 30 negative supercoils, is consistent with the lack of observed activity on (−)sc DNA. At a 20-fold higher Topo IV concentration, the authors reported distributive relaxation of negative supercoils occurring at a rate of ≈8 strand passages per min (6). Under the assumption of a pseudo-first-order binding rate $k_b = k_1$[Topo IV], the model predicts a relaxation rate for negative supercoils of 4–5 strand passages per min. Given the large uncertainty in estimating t_b and the possibility of multiple Topo IV acting at the higher enzyme concentration, this discrepancy is reasonable. In single-molecule measurements of the relaxation of braided DNA molecules by Topo IV, the asymmetry was determined to be near complete (4, 7). In these experiments, the number of DNA crossings varied from 40 to 200. Assuming $t_w \approx 50$ s, R ranges from 95 ± 10 to 300 ± 30. These asymmetry values imply relaxation times for right-handed braids between 3 and 15 h, again consistent with the claims of absolute preference for positive supercoiled DNA.

Kinetic Competition and Processivity. We consider an arbitrary step in an enzymatic cycle at which the enzyme can dissociate, with rate k_{off}, or continue to the next step, with rate k_{for}. The probability of dissociating $P_{off} = k_{off}/(k_{off} + k_{for})$, and the probability of completing the cycle is $P_{for} = k_{for}/(k_{for} + k_{off})$. The processivity of the enzyme, i.e., the average number of cycles completed per binding event, can be calculated from P_{for}. The probability of completing exactly n cycles before unbinding is $P(n) = (1 - P_{for})\cdot(P_{for})^n$. To compute the average number of cycles per binding event, we sum over all possible number of cycles weighted by the probability of completing n cycles

$$\langle n \rangle = \sum_{n=1}^{\infty} n(1 - P_{for})(P_{for})^n = \frac{P_{for}}{(1-P_{for})} \qquad [s1]$$

where we have made use of the result known as Gabriel's staircase,

$$\sum_{n=1}^{\infty} nr^n = \frac{r}{(1-r)^2}, r < 1. \qquad [s2]$$

Thus, processivity is given by $P_{for}/(1 - P_{for})$. For example, $P_{for} = 0.5$ results in a processivity of 1. However, the probability of completing more than one cycle is equal to the probability of completing a single cycle, which would be reflected in the distribution of the number of cycles completed per binding event. The mean of the distribution would be 1, but there would be as many multiple turnover events as single turnover events. As the processivity decreases, the relative probability of completing a single step, rather than multiple steps, increases. The processivity of Topo IV on (−)sc DNA is so small that all of the ≈500 relaxation cycles we observed occurred in individual steps of one strand passage (Fig. 4*C Inset*). It is impossible to calculate the processivity based on this measurement; however, we can calculate a conservative estimate of the upper bound for the processivity by assuming that the probability of not observing a multiple relaxation event during 500 single cycles was 5%. Under this assumption, the probability $P(n > 1)$ of two or more successive strand passages is 0.006, which is calculated from the binomial probability function $0.05 = (1 - P)^{500}$. The probability of observing more than one cycle is $P(n > 1) = (P_{for})^2$, which is calculated from the geometric series for $P(n)$ above. The resulting upper boundary on P_{for-} is 0.08 with 0.95 confidence, which results in a processivity on (−)sc DNA not >0.08. However, the processivity on (+)sc DNA is ≈40, resulting in a P_{for+} of ≈0.98. Comparison of these two probabilities suggests at least a 600-fold difference between k_{for+} and k_{for-}, under the assumption that k_{off} is the same for both (+)sc and (−)sc DNA.

Mechanistic Model for Topo IV Processivity. Supercoil relaxation data (Fig. 4) suggest that the preferential relaxation of positive supercoils is caused primarily by the increased processivity of Topo IV on (+)sc DNA. Models describing the activity of Topo IV must therefore account for the highly processive relaxation of positive supercoils and the perfectly distributive relaxation of negative supercoils. We suggest that this dramatic difference in processivity arises from a kinetic competition between T segment rebinding and G segment release after the first-strand passage reaction. The kinetic competition most likely occurs

during the large DNA conformational changes that accompany the refolding of the DNA subsequent to the initial strand passage. We propose a model based on this hypothesis (Fig. S4*B*) that couples the established enzymatic cycle of Topo IV (3, 9, 10) (see also Fig. S1) and recent results implicating the C-terminal domains (CTDs) in chiral discrimination (11, 12) with the structure and dynamics of supercoiled DNA.

In the model presented in Fig. S4*B*, Topo IV first binds the G segment at the end of the plectoneme (see main text) possibly facilitated by the increased conformational flexibility or the apical bend of the distal loop. This is consistent with electron micrographs showing Topo IV bound to the end of plectonemes (13) and by single-molecule force-induced unbinding experiments demonstrating that Topo IV specifically stabilizes the distal loop in a plectoneme (14). Capture of the T segment occurs at a crossing angle of ≈85°, which may also be facilitated by the flexibility of the distal DNA loop. Once the T segment is captured, ATP binding, clamp closure, strand passage, and religation occur rapidly ($\approx 2.5\ s^{-1}$) for both positive and negative supercoils (4, 6, 7), changing the linking number by 2 and generating a loop of locally unwound DNA. On (+)sc DNA, Topo IV remains bound to the loop, imposing a slight bend and twist, both of which favor positive supercoiling (14). The CTDs of Topo IV may participate in the bending (12) and twisting of the DNA and likely stabilize the enzyme on the DNA during the refolding process (11). The loop is highly unstable, and it quickly collapses, reforming two supercoils at the expense of two supercoils at the proximal end of the plectoneme. From the high-energy configuration the DNA loop collapses to the lowest-energy configuration, which, because of the binding energy of Topo IV, is a slightly distorted supercoil in which the DNA is correctly positioned for strand passage, i.e., with a crossing angle of ≈85°. Productive binding geometry is therefore rapidly reestablished after each strand passage, resulting in processive relaxation. Processivity is enhanced because Topo IV binds the distal end of the plectoneme, which is reformed after each strand passage until the plectoneme is completely relaxed. If binding were to occur randomly along the plectoneme, only the supercoils between the initial binding site and the proximal end of the plectoneme would be relaxed, which would reduce the effective processivity.

On (−)sc DNA we propose that subsequent to strand passage, the twist and bend imposed by Topo IV which favor positive supercoiling hinder the reformation of negative supercoils. Furthermore, the orientation of the C-terminal domains (CTDs) may result in weak or no stabilization of the enzyme during the refolding of the negative plectoneme (Fig. S4*B*), causing an increased off-rate. The combination of reduced plectoneme-refolding rate and the increase in off-rate effectively eliminates the possibility of catalyzing a second reaction, rendering the reaction distributive. As a result, the processivity is exceedingly low, and relaxation of negative supercoils progresses in steps of one strand passage per binding event, as observed (Fig. 4 *B* and *C*).

Monte Carlo Simulations. Details of the MC simulations have been published (4, 15, 16). Briefly, two 1.2-μm (3.6-kb) DNA molecules a distance $2e$ apart, were modeled as self-avoiding discrete worm-like chains. The ratio of tether separation to tether length ($2e/L$) was set to the experimentally determined value. A metropolis MC algorithm was used to generate distributions of chain conformations satisfying topological constraints. When the separation between the two DNA chains was less than a threshold distance (10 nm), a juxtaposition event was considered to take place, and the angle formed by the two segments of closest approach was calculated. Typically, the angular probability distribution function was computed from 10^9 chain configurations for each force and $2e/L$ value. Because the ratio of the probability distribution functions of left- and right-handed crossings under otherwise identical conditions was used to compute the preferred crossing angles, the results are insensitive to linear errors in the calculated probability distributions. The computed crossing angle results were robust against perturbations of the input parameters, *e.g.*, 10–15% variation in force, $2e/L$, or separation threshold did not significantly alter the computed crossing angle.

1. Roca J, Wang JC (1996) The probabilities of supercoil removal and decatenation by yeast DNA topoisomerase II. *Genes Cells* 1:17–27.
2. Trigueros S, Salceda J, Bermudez I, Fernandez X, Roca J (2004) Asymmetric removal of supercoils suggests how topoisomerase II simplifies DNA topology. *J Mol Biol* 335:723–731.
3. Champoux JJ (2001) DNA topoisomerases: Structure, function, and mechanism. *Annu Rev Biochem* 70:369–413.
4. Stone MD, et al. (2003) Chirality sensing by *Escherichia coli* topoisomerase IV and the mechanism of type II topoisomerases. *Proc Natl Acad Sci USA* 100:8654–8659.
5. Vologodskii A, Cozzarelli NR (1996) Effect of supercoiling on the juxtaposition and relative orientation of DNA sites. *Biophys J* 70:2548–2556.
6. Crisona NJ, Strick TR, Bensimon D, Croquette V, Cozzarelli NR (2000) Preferential relaxation of positively supercoiled DNA by *E. coli* topoisomerase IV in single-molecule and ensemble measurements. *Genes Dev* 14:2881–2892.
7. Charvin G, Bensimon D, Croquette V (2003) Single-molecule study of DNA unlinking by eukaryotic and prokaryotic type II topoisomerases. *Proc Natl Acad Sci USA* 100:9820–9825.
8. Hiasa H, Marians KJ (1996) Two distinct modes of strand unlinking during θ-type DNA replication. *J Biol Chem* 271:21529–21535.
9. Wang JC (2002) Cellular roles of DNA topoisomerases: A molecular perspective. *Nat Rev Mol Cell Biol* 3:430–440.
10. Corbett KD, Berger JM (2004) Structure, molecular mechanisms, and evolutionary relationships in DNA topoisomerases. *Annu Rev Biophys Biomol Struct* 33:95–118.
11. Corbett KD, Schoeffler AJ, Thomsen ND, Berger JM (2005) The structural basis for substrate specificity in DNA topoisomerase IV. *J Mol Biol* 351:545–561.
12. Corbett KD, Shultzaberger RK, Berger JM (2004) The C-terminal domain of DNA gyrase A adopts a DNA-bending β-pinwheel fold. *Proc Natl Acad Sci USA* 101:7293–7298.
13. Vologodskii AV, et al. (2001) Mechanism of topology simplification by type II DNA topoisomerases. *Proc Natl Acad Sci USA* 98:3045–3049.
14. Charvin G, Strick TR, Bensimon D, Croquette V (2005) Topoisomerase IV bends and overtwists DNA upon binding. *Biophys J* 89:384–392.
15. Vologodskii AV, Cozzarelli NR (1994) Conformational and thermodynamic properties of supercoiled DNA. *Annu Rev Biophys Biomol Struct* 23:609–643.
16. Charvin G, Vologodskii A, Bensimon D, Croquette V (2005) Braiding DNA: Experiments, simulations, and models. *Biophys J* 88:4124–4136.

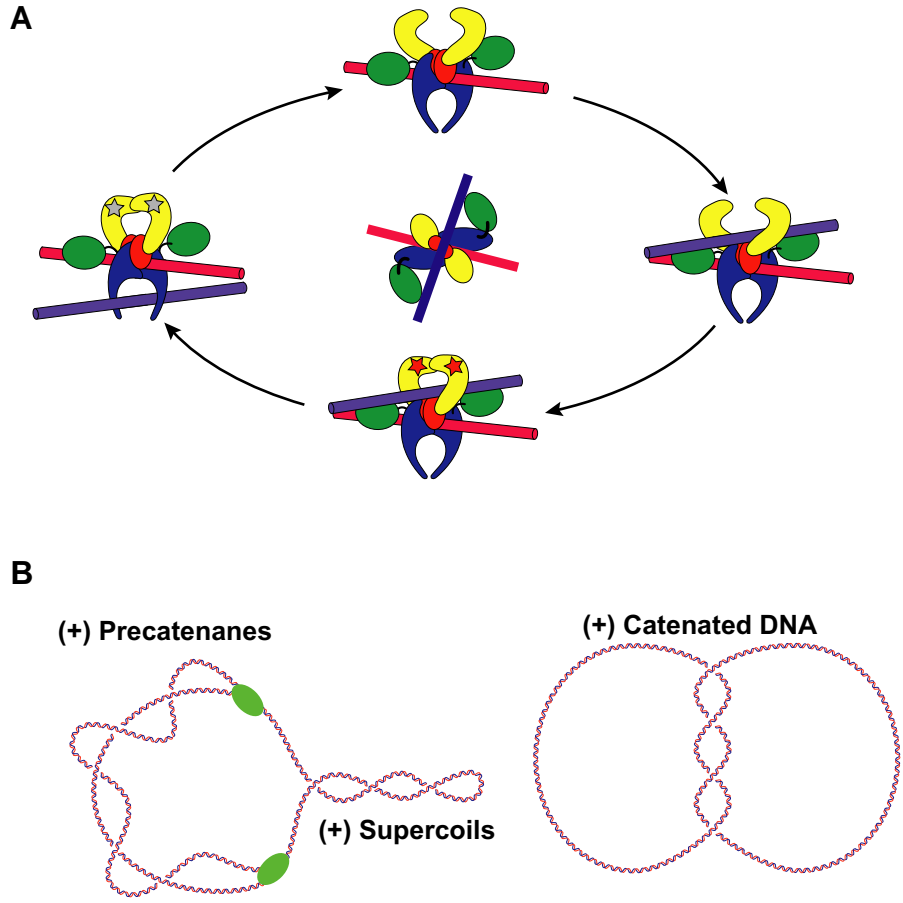

Fig. S1. Topo IV biochemical cycle and in vivo activity. (*A*) Diagram and biochemical cycle of Topo IV. The domains of the Topo IV heterotetramer ($ParC_2$:$ParE_2$) are colored according to function. The DNA-binding domains are red, the cleavage domains are blue, the ATPase domains are yellow, and the ParC CTDs are green. The model and color scheme are adapted from Corbett et al. (11). Topo IV binds the gate (G) segment of DNA (red), followed by binding of the transfer (T) segment (blue). Subsequent binding of ATP (red stars) closes the top gate (yellow domains), followed by G segment cleavage, T segment passage, and hydrolysis of ATP. Opening the bottom clamp (blue domains) releases the T segment, changing the linking number by 2. Release of ADP (gray stars) resets the enzyme. The center diagram depicts a top-down view of Topo IV, illustrating the putative role of the ParC CTDs in orienting the T and G segments and imposing the preferred crossing angle. (*B*) In vivo roles of Topo IV. DNA undergoing replication (green ovals represent replication complexes) develops positive supercoils ahead of the replication forks and positive precatenanes behind. The crossing angles in positively supercoiled DNA are $<90°$, whereas they are $>90°$ in the positive precatenanes. Topo IV can unlink precatenanes and remove positive supercoils. If precatenanes are not removed during replication, the replicated DNA molecules are catenated and must be separated by Topo IV.

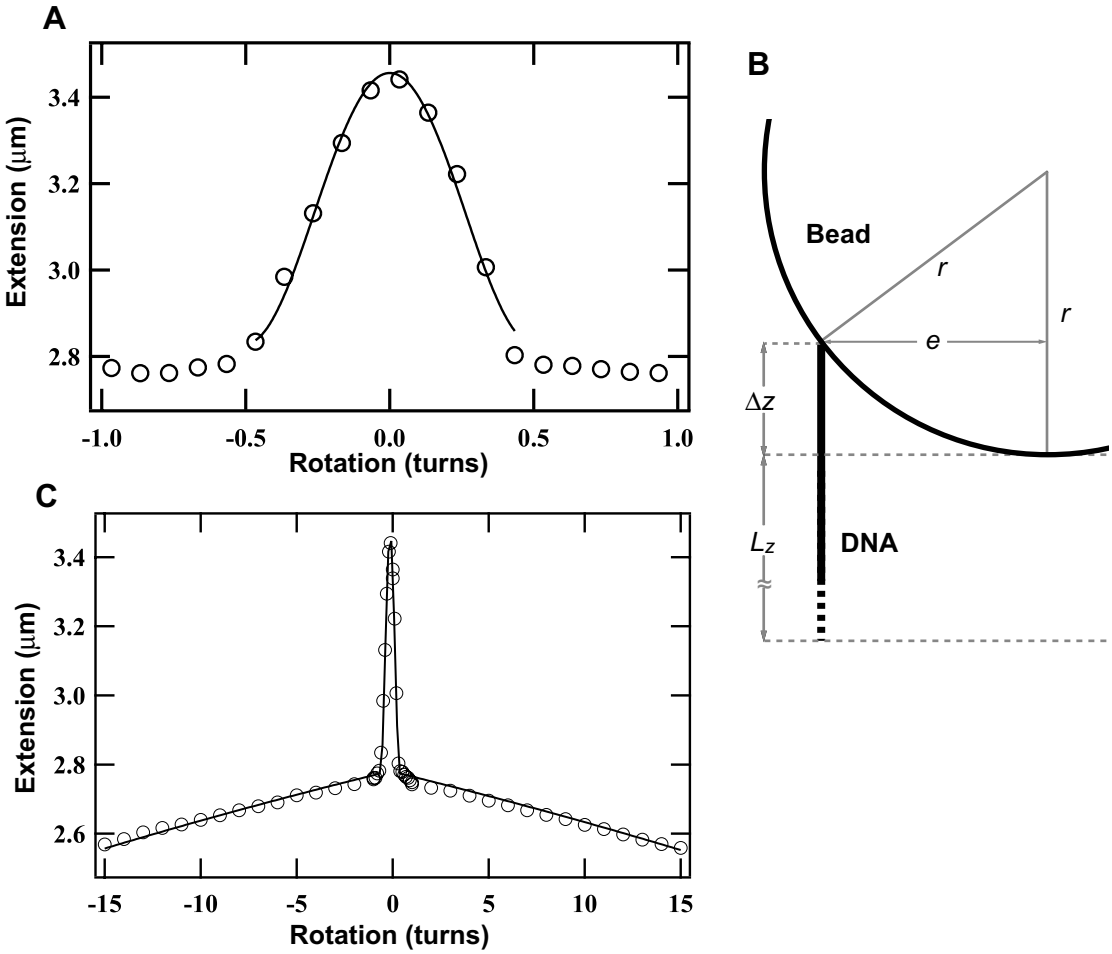

Fig. S2. Geometric fits to double tether extension versus rotation curve. (*A*) Extension as a function of rotation for a double tether (open circles) near 0 turns. For rotations between 0 and ± 0.5 turns the extension decreased rapidly and was well fit by a geometric model (7) (line):

$$L = \sqrt{L_0^2 - 4e^2 \sin^2(n\pi)} - r + \sqrt{r^2 - e^2},\ |n| < 0.5 \qquad \textbf{[s3]}$$

where L is the measured extension, L_0 is the maximum extension, e is the half-separation distance between the DNA molecules, n is the number of rotations, and r is the radius of the bead. The first term in the expression describes the extension of a twisted swing. The second two terms are a correction for the spherical bead. (*B*) Origin of correction terms for spherical bead. The second two terms in the expression are necessary to account for the segment of DNA (Δz in the figure) between the point of attachment and the lower edge of the bead, which is the reference point for extension measurements. The experimentally measured extension is L_z, which does not include the short length of DNA, Δz. To compare the fitted value of the DNA length with the actual length of the DNA used to prepare the tethers, a correction must be applied to account for Δz. Note that the correction does not introduce additional free parameters because the radius of the bead is fixed. The fit returned the DNA length L_0 and the distance between the DNA molecules 2e. If L_0 is equal to the expected DNA length, the tether geometry is parallel. If, however, the tether geometry is trapezoidal, L_0 will be less than the DNA length. More complicated tether geometries, such as triple tethers, lead to asymmetric or trapezoidal tethers, which were not used. As a final check on the tether geometry, the slope of the DNA segment attached to the bead at a half-rotation was compared with the slope of the tangent to the bead at the point of attachment. The tether was used only if the slope of the DNA segment was greater than the slope of the tangent, which ensured that the DNA did not partially wrap around the bead at rotations >0.5. (*C*) Rotation extension relation for double tether at larger rotations. Extension as a function of rotation for rotations up to ± 15, including the data from part *a* (densely spaced points near 0 rotation). For $|n| > 0.5$, the extension decreased slowly with applied turns as the DNA molecules twisted around each other (16). This part of the curve is well fit by a geometric winding model (7, 16):

$$L = \sqrt{L_0^2 - (2e + \pi D_e(|n| - \tfrac{1}{2}))^2} - r + \sqrt{r^2 - e^2},\ |n| > 0.5 \qquad \textbf{[s4]}$$

where we have introduced the effective DNA diameter D_e (16). Fitting the high rotation data provided a second means of testing the double tether. For triple tethers, the D_e parameter was approximately twice as large as it was for double tethers. These tethers were rejected, as were tethers that were asymmetric with respect to rotation. The line represents a simultaneous fit to both functions defined over the regions $|n| < 0.5$ and $|n| > 0.5$. The parameter e was used as an input for the MC simulations.

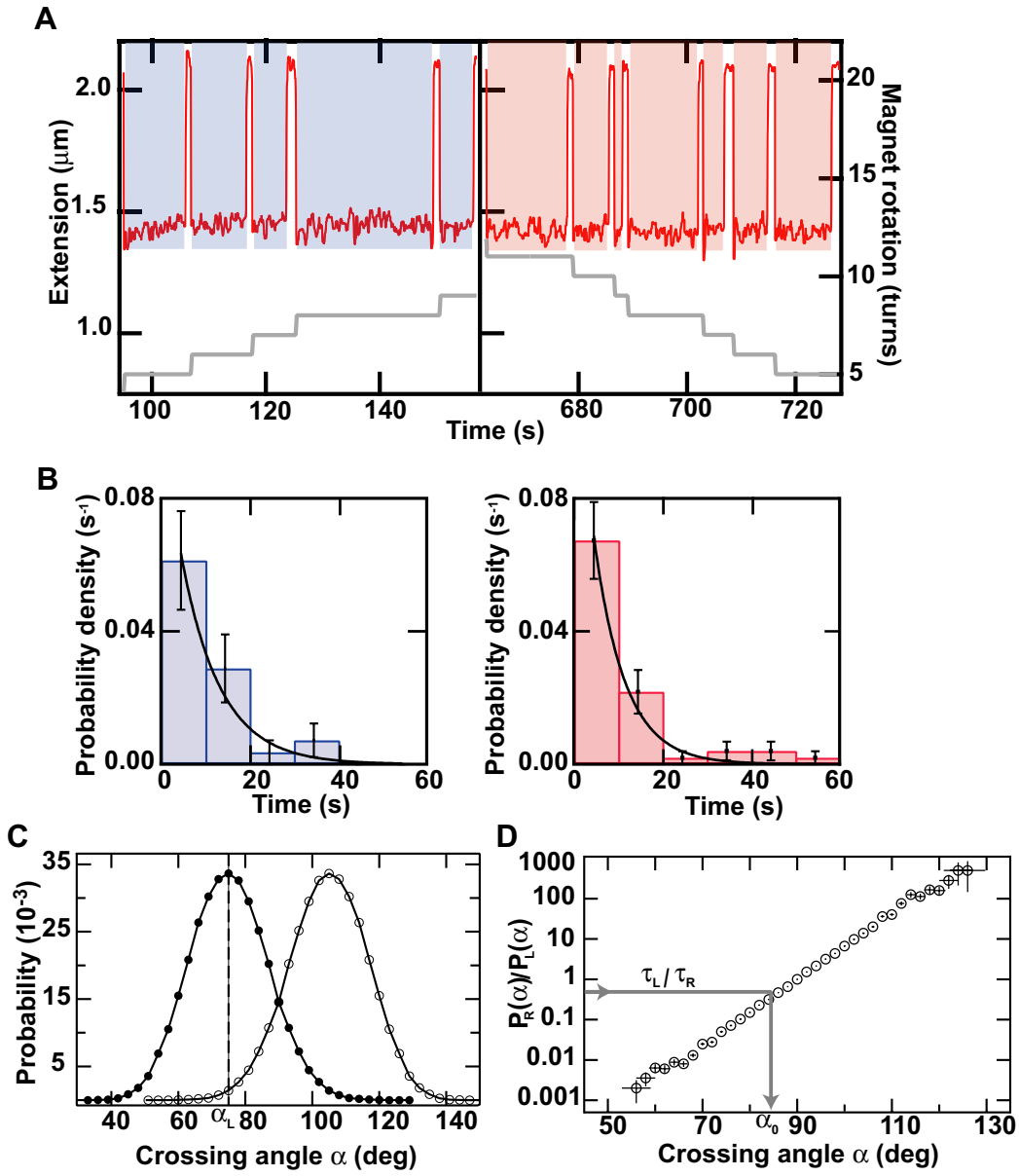

Fig. S3. Relaxation of a nearly symmetric single crossing. Figs. 1 and 3 in the main text display the data and MC simulations for a single DNA crossing with a small, narrowly distributed, left-handed crossing angle α_L, which resulted in highly asymmetric relaxation of the left- and right-handed crossings. This figure displays the data and MC simulations for a single DNA crossing with a large, broadly distributed, left-handed crossing angle α_L, which resulted in nearly symmetric relaxation of the left- and right-handed crossings. (*A*) Extension (red line) and magnet rotation (gray line) as a function of time, as depicted in Fig. 1. The DNA tether length was 3.5 μm, the separation between tethers was 1.76 μm, and the force was 0.4 pN. (*Left*) Introduction and relaxation of right-handed crossings. The time to relax each crossing is indicated by the blue shading. (*Right*) Relaxation of left-handed crossings for the same molecule at the same protein concentration, with the time to relax each crossing indicated by red shading. (*B*) Distributions of relaxation times. Single exponential fits to the distributions of right-hand crossing relaxation times (*Left*, blue bars $\tau_R = 6.9 \pm 1.2$ s, $\chi^2_\nu = 1.4$) and of left-hand crossings (Right, red bars $\tau_L = 8.7 \pm 2.1$ s, $\chi^2_\nu = 1.2$) are shown. The ratio of relaxation times was $\tau_R/\tau_L = 0.8 \pm 0.2$. (*C*) Probability distributions for single left- (filled circles) and right-handed (open circles) crossings for this tether geometry and force computed via MC simulations. The peak of the probability distribution was 76°. (*D*) Ratio of right- to left-handed probability distributions from *c*. The preferred crossing angle was given by the angle at which the ratio was equal to the measured asymmetry, 0.8 ± 0.2, which gave $\alpha_0 = 88.5 \pm 1.5°$.

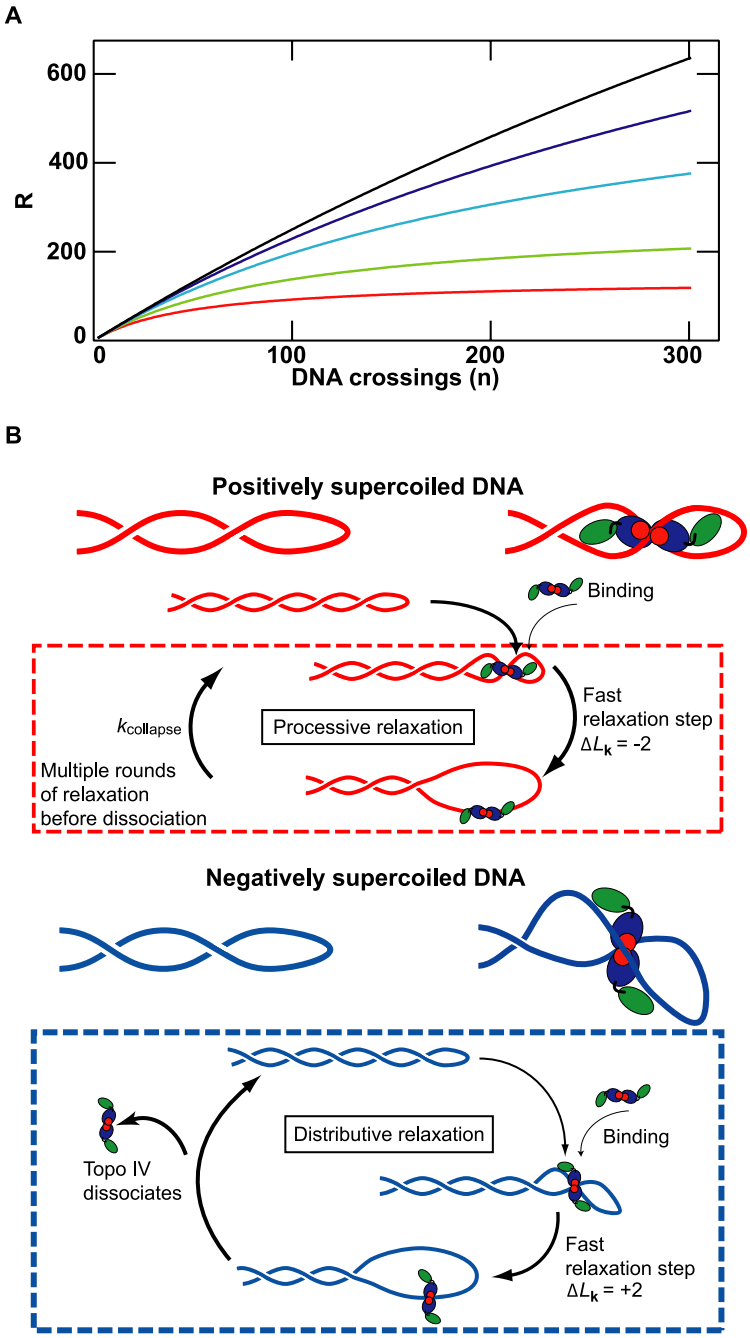

Fig. S4. Model of supercoil relaxation by Topo IV. (*A*) Quantitative model of supercoil relaxation by Topo IV. Calculated values of the asymmetry parameter *R* (see *Results and Discussion*) are plotted as a function of the number of DNA crossings. Each curve corresponds to a different average binding time (t_b) on (+)sc DNA: 200 s (black), 100 s (blue), 50 s (cyan), 20 s (green), 10 s (red). (*B*) Mechanistic model for Topo IV relaxing (+)sc and (−)sc DNA. (*Top*) (+)sc DNA in which the crossing angle of juxtaposed DNA segments is ≈60° (*Left*, drawn to scale). Topo IV (blue, catalytic core; green, ParC-CTD; red, clamp) productively binds the juxtaposed DNA segments with an opening angle of ≈85° at the distal end of the plectonemic structure (*Right*). Once Topo IV is productively bound, strand passage, which decreases the linking number by 2, occurs quickly, resulting in the generation of an unstable loop of DNA. Topo IV remains bound to the loop, likely stabilized by the CTDs, imposing a slight bend and twist that favor positive supercoiling (14). The loop rapidly collapses by forming a positive supercoil around the Topo IV, which reestablishes the correct DNA juxtaposition geometry. The newly formed supercoil is quickly relaxed, and the cycle repeats, resulting in processive relaxation of positive supercoils (red dashed box). (*Bottom*) Relaxation of (−)sc DNA in which the crossing angle of juxtaposed DNA segments is ≈120° (*Left*). Topo IV productively binds the juxtaposed DNA segments with an opening angle of ≈85° at the distal end of the plectonemic structure (*Right*). The binding step is slower on (−)sc DNA compared with (+)sc DNA because of the larger angular fluctuation required. Once Topo IV productively binds the DNA crossing, strand displacement takes place, resulting in the formation of a loop of DNA. In this case, the binding energy of Topo IV frustrates the reformation of a productively bound conformation. Additionally, the CTDs are not correctly positioned to stabilize the protein on the DNA during the large conformational change. As a result, Topo IV unbinds before the reformation of the negative supercoils. The cycle begins again with a slow binding step before the next strand passage can take place, which results in distributive relaxation of negative supercoils (blue dashed box).